

Conductivity studies of poly(ethylene oxide)(PEO)/poly(vinyl alcohol) (PVA) blend gel polymer electrolytes for dye-sensitized solar cells

T. S. Tiong¹ · M. H. Buraidah¹ · L. P. Teo¹ · A. K. Arof¹

Received: 21 February 2016 / Revised: 18 April 2016 / Accepted: 8 June 2016 / Published online: 20 June 2016
© Springer-Verlag Berlin Heidelberg 2016

Abstract Poly(ethylene oxide)(PEO)–poly(vinyl alcohol) (PVA) blend-based gel polymer electrolytes (GPEs) have been prepared by blending equal weights of PEO and PVA in ethylene carbonate (EC), dimethyl sulfoxide (DMSO), tetrabutylammonium iodide (TBAI), and iodine crystals (I₂). The conductivity, diffusion coefficient, number density, and ion mobility of the electrolytes have been calculated from the impedance data obtained from electrochemical impedance spectroscopy (EIS) measurements. The GPE with the composition of 7.02 wt%, PVA, 7.02 wt% PEO, 30.11 wt% ethylene carbonate (EC), 30.11 wt% DMSO, 24.08 wt% TBAI and 1.66 wt% I₂ exhibits the highest conductivity of 5.5 mS cm⁻¹ at room temperature. Dye-sensitized solar cells (DSSCs) with configuration fluorine tin oxide (FTO)/titanium dioxide/N3-dye/GPE/platinum/FTO have been fabricated and tested under the white light of intensity 100 mW cm⁻². The DSSC containing the highest conducting GPE exhibits the highest power conversion efficiency, η of 5.36 %.

Keywords Poly(ethylene oxide) (PEO) · Poly(vinyl alcohol) (PVA) · Gel polymer electrolyte · Dye-sensitized solar cells

Introduction

Dye-sensitized solar cell (DSSC) was first reported by O'Regan and Grätzel in 1991 [1]. DSSCs can be manufactured from

simple preparation methods and low-cost materials; therefore, their production cost is low [2]. DSSCs are based on nanostructured mesoscopic materials, and they are produced from either organic materials or mixtures of organic and inorganic materials. The mesoscopic characteristic of the DSSCs enables them to be made into transparent cells, which can be used to produce photovoltaic windows. DSSCs also have the advantage of attaining higher efficiency under lower light intensity [3]. Although the maximum attainable efficiency of DSSCs is lower than that of silicon-based solar cells [4, 5], DSSC is still considered as an attractive candidate for a widely commercialized solar cell due to its characteristics discussed above. Since DSSC was first reported in 1991 [1], research on DSSCs has intensified throughout the world.

A DSSC contains an electrolyte as one of its components. The electrolyte is in contact with the dye, and its function is to restore the dye after the dye has been oxidized. The electrolyte can be a liquid electrolyte (LE), a solid polymer electrolyte (SPE), or a gel polymer electrolyte (GPE). Conventional LE has shown high efficiency of the DSSC, but the problem with conventional LE is that it does not last long as it can evaporate and leak [6]. On the other hand, SPE can overcome the evaporation and leakage problems, but its demerit is having poor contact at the electrolyte/electrode interface, resulting in low efficiency [7]. GPE is currently the most promising substitution for SPE and conventional LE due to its properties such as good ionic conductivity, good interfacial filling property, good thermal stability, good long-term stability, ability to interact with the titanium dioxide (TiO₂) electrode, does not leak easily, simple to prepare, and lower in price compared to ionic liquid [8, 9].

Many types of polymers have been applied in the polymer electrolyte systems for DSSCs, including

✉ M. H. Buraidah
mhburaidah@um.edu.my

¹ Department of Physics, Faculty of Science, Centre for Ionics University of Malaya, 50603 Kuala Lumpur, Malaysia

polyacrylonitrile (PAN) [10], poly(vinylidene fluoride) (PVDF) [11], poly(vinylidene fluoride–poly(methyl methacrylate) (PVDF-PMMA) [12], poly(ethylene oxide)–poly(methyl methacrylate) (poly(ethylene oxide)(PEO)-PMMA) [13], and poly(vinyl butyral (PVB) [14], to name a few. These polymers have been mixed with various salts to provide ions for conduction. PEO and poly(vinyl alcohol) (PVA) are some polymers that have been used for application in DSSCs [15, 16]. Table 1 shows some publications representing the state of the art on DSSCs with GPEs. It can be noted that the efficiency of DSSCs with gel polymer electrolytes is still lower than DSSCs using liquid electrolytes ($\eta \sim 13\%$) [22]. Therefore, understanding of transport properties of GPEs and charge transfer process in DSSCs is important in order to improve the performance of DSSCs.

PC propylene carbonate, *EC* ethylene carbonate, *DMC* dimethyl carbonate, *TBP* tert-butylpyridine, *NaI* sodium iodide, *Li* lithium iodide, *Pr₄NI* tetrapropylammonium iodide

It is known from literature that polymer electrolytes with blended polymers exhibit better properties compared to the electrolytes using single polymer host [23]. Therefore, by blending PVA and PEO in a polymer electrolyte, better properties are expected to be exhibited. PEO has the advantage to solvate a variety of salts in high concentrations [24], whereas PVA is non-toxic and adhesive and has good film-forming ability [25, 26]. Joge et al. [27] have investigated PEO-PVA (1:1 ratio)–silver nitrate–aluminum oxide SPE via electrochemical impedance spectroscopy (EIS), differential scanning calorimetry (DSC), and X-ray diffraction (XRD), whereas El-kader et al. [28] studied the structural and thermal properties of PEO-PVA (1:1 ratio)–titanium dioxide SPE. However, to the best of the authors' knowledge, there is no report on the utilization of PEO-PVA-blended GPEs in DSSCs available from the literature. In this work, following the reports in [27] and [28], blended gel polymer electrolytes containing equal weights of PEO and PVA have been used in DSSC. The aim of this work is to study the ionic transport properties of PEO-PVA GPEs in terms of number

density, ionic mobility, and diffusion coefficient for better understanding in conductivity and DSSC's performance.

Experimental

Electrolyte preparation

Firstly, 0.21 g of PVA (Aldrich), 0.21 g of PEO (Aldrich), and 0.90 g of EC (Aldrich) were dissolved in 0.90 g of dimethyl sulfoxide (DMSO) (Friendemann Schmidt). DMSO is chosen as a solvent because it is an excellent solvent for polar compounds, having high boiling point (462 K), and is less toxic than other members in its class, such as dimethylformamide, dimethylacetamide, *N*-methyl-2-pyrrolidone, and hexamethylphosphoramide [29]. Eight of these solutions were prepared. Different amounts (0.12, 0.24, 0.36, 0.48, 0.60, 0.72, 0.84, and 0.96 g) of tetrabutylammonium iodide (TBAI) (Aldrich) were added into each solution. The solutions were then heated to 383 K and stirred until viscous gel-like solutions were formed. The gels were then allowed to cool down to 325 K. Iodine crystals (Amco Chemie) (6.90 % mass of TBAI) were added into each solution, and the solutions were stirred until homogenous gel polymer electrolytes were obtained. The compositions of the electrolytes and their designation are tabulated in Table 2.

The impedance of each sample was determined by EIS. The measurements were performed using the Hioki 3531 Z Hi Tester in the frequency range from 50 Hz to 5 MHz at temperatures between 303 and 363 K. The ionic conductivity, σ , of each sample was then calculated from the equation below:

$$\sigma = \frac{t}{R_b A} \quad (1)$$

where A is the area and t is the thickness of the samples. R_b is the bulk resistance of the samples, which can be obtained from the complex impedance plot.

Table 1 Literature of DSSCs using gel polymer electrolytes

| | Conductivity (mS cm ⁻¹) | Open-circuit voltage (V) | Short-circuit current density (mA cm ⁻²) | Fill factor | Efficiency (%) | Ref |
|----------------------------------------------|-------------------------------------|--------------------------|------------------------------------------------------|-------------|----------------|------|
| PVDF-PC-EC-NaI/I ₂ | 2.34 | 0.58 | 5.82 | 0.39 | 1.32 | [17] |
| PEO-EC/PC-LiI/I ₂ | 5.20 | 0.58 | 2.80 | 0.60 | 3.60 | [18] |
| PMMA-EC/PC/DMC-NaI/I ₂ | 6.89 | 0.78 | 10.07 | 0.61 | 4.78 | [19] |
| PEO/PMMA-LiI/I ₂ -TBP/EC/PC | 7.00 | 0.76 | 11.11 | 0.58 | 4.90 | [20] |
| PVDF-EC-PC-Pr ₄ NI/I ₂ | 4.38 | 0.68 | 6.15 | 0.69 | 2.90 | [21] |

Table 2 The composition of the GPEs and their designation

| Sample | Electrolyte composition |
|--------------|--------------------------------------------------------------------------------------------------------|
| Without salt | 8.94 wt% PEO - 8.94 wt% PVA - 38.33 wt% EC - 38.33 wt% DMSO |
| A | 8.94 wt% PEO - 8.94 wt% PVA - 38.33 wt% EC - 38.33 wt% DMSO - 5.11 wt% TBAI - 0.35 wt% I ₂ |
| B | 8.48 wt% PEO - 8.48 wt% PVA - 36.34 wt% EC - 36.34 wt% DMSO - 9.69 wt% TBAI - 0.67 wt% I ₂ |
| C | 8.06 wt% PEO - 8.06 wt% PVA - 34.55 wt% EC - 34.55 wt% DMSO - 13.82 wt% TBAI - 0.96 wt% I ₂ |
| D | 7.68 wt% PEO - 7.68 wt% PVA - 32.93 wt% EC - 32.93 wt% DMSO - 17.56 wt% TBAI - 1.22 wt% I ₂ |
| E | 7.34 wt% PEO - 7.34 wt% PVA - 31.46 wt% EC - 31.46 wt% DMSO - 20.97 wt% TBAI - 1.43 wt% I ₂ |
| F | 7.02 wt% PEO - 7.02 wt% PVA - 30.11 wt% EC - 30.11 wt% DMSO - 24.08 wt% TBAI - 1.66 wt% I ₂ |
| G | 6.74 wt% PEO - 6.74 wt% PVA - 28.87 wt% EC - 28.87 wt% DMSO - 26.94 wt% TBAI - 1.84 wt% I ₂ |
| H | 6.47 wt% PEO - 6.47 wt% PVA - 27.73 wt% EC - 27.73 wt% DMSO - 29.57 wt% TBAI - 2.03 wt% I ₂ |

DSSC assembly

Fluorine-doped tin oxide (FTO) glass substrates (Solaronix) were cleaned with distilled water, diluted sulfuric acid (Friendemann Schmidt), and acetone (Friendemann Schmidt). Two layers of titanium dioxide (TiO₂) with different particle sizes were deposited on the FTO glass for preparing the photoanode. For the first layer, 0.5 g of TiO₂-P90 powder (particle size 15.9 nm) from Evonik Industries was ground in 2 mL dilute nitric acid (Friendemann Schmidt) before being spin-coated on FTO glasses. The TiO₂-coated FTO glasses were then sintered at 723 K for 30 min. For the second layer, 0.5 g of TiO₂-P25 powder (particle size 21 nm) from Evonik Industries and 0.1 g carbowax (Aldrich) were added into 2 mL of nitric acid and the mixture was ground for about 60 min. A few drops of surfactant (Triton-X from Aldrich) were added to the TiO₂ paste, which was then coated on the top of the first TiO₂ layer on the FTO glass by doctor blade method. The second layer-coated electrodes were then sintered at 723 K for 30 min. The thickness of the TiO₂ layer was around 50 μm. The double-layer-coated TiO₂ electrode was then soaked in 0.3 mM N3 dye (Solaronix) for 24 h for dye adsorption.

The DSSCs were fabricated by sandwiching the GPEs between the TiO₂ photoelectrode and platinum (Pt) counter electrode to have the configuration FTO/TiO₂/N3 dye/GPE/Pt/FTO. The *J-V* characteristics of the DSSCs were measured under white light intensity of 100 mW cm⁻² (1.5 AM) using a solar simulator instrument (Oriol LCS-100). The active area of the cells was 0.196 cm² (the area of mask used). EIS of the fabricated cells was also

measured under same intensity with frequency range from 100 kHz to 10 mHz with the bias voltage set at open-circuit voltage using potentiostat (Autolab PGSTAT 128 N).

Results and discussion

Ionic conductivity of the GPEs

Figure 1 shows the Nyquist plots of selected blended PEO-PVA gel polymer electrolytes at 303 K. The presence of the spike in the Nyquist plots indicates that the charge carriers are ions and the total conductivity is mainly the result of ionic conduction [30]. The impedance behavior of the GPEs can be represented by the equivalent circuit as shown in Fig. 1, which consists of a resistor connected in series with a constant phase element (CPE). The equation of the real and imaginary impedances of the equivalent circuit can be expressed as follows [31]:

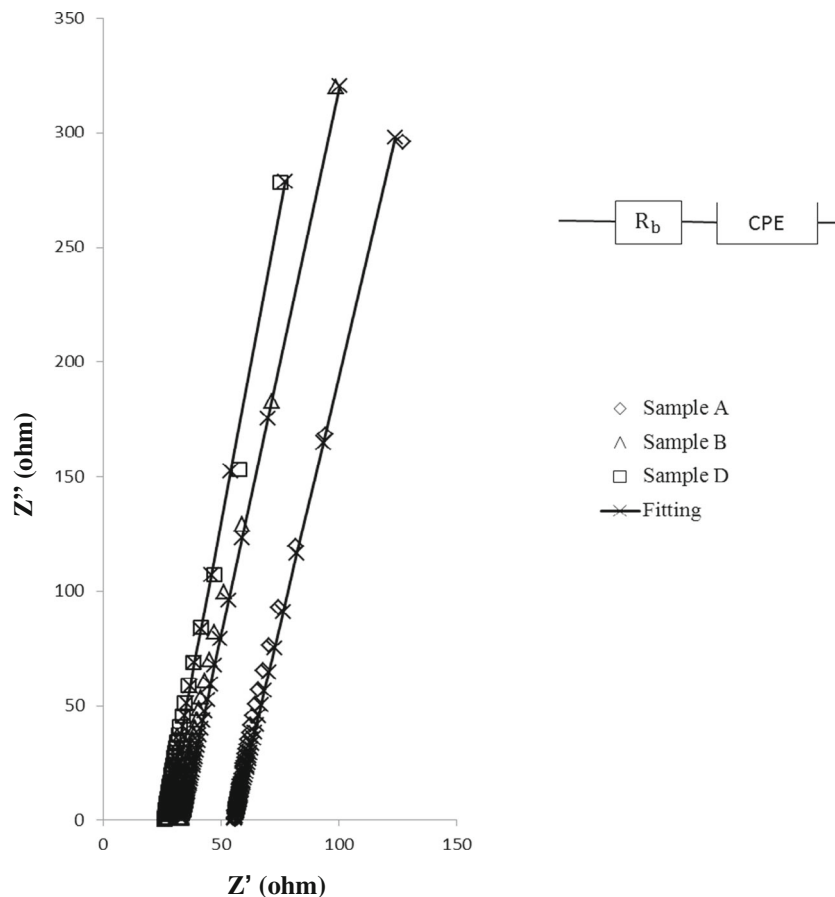
$$Z' = R_b + \frac{\cos\left(\frac{\pi p}{2}\right)}{k^{-1}\omega^p} \quad (2)$$

$$Z'' = \frac{\sin\left(\frac{\pi p}{2}\right)}{k^{-1}\omega^p} \quad (3)$$

where Z' and Z'' are the real and imaginary parts of impedance, respectively, k^{-1} corresponds to value of capacitance of CPE, R_b is the bulk resistance of the sample, ω (which is equal to $2\pi f$, where f is the frequency) is the angular frequency, and p is the fraction of right angle that the spike makes with the horizontal axis in the Nyquist plot. CPE behaves like a leaky capacitor. The values of k^{-1} and p are listed in Table 3. The capacitance values, k^{-1} , obtained in this work are found to be in the range of microfarad, which are comparable with the results reported by Ramya and co-workers [32]. As can be observed from Table 3, the values of p are less than 1 since all the spikes in Fig. 1 are tilted at an angle less than 90°, and this indicates that the GPEs have both resistive and capacitive behaviors. As can be seen from the Nyquist plots in Fig. 1, there is a good fit between the experimental data (represented as symbols) and the fitting line (from the formula of Z' and Z'' in Eqs. (2) and (3)), indicating that the equivalent circuit well described the GPE system.

Figure 2 shows the variation of ionic conductivity of GPEs with TBAI concentration at 303 K. As can be seen from the graph and Table 3, the conductivity increases from 1.9 mS cm⁻¹ until a maximum value was reach at 5.5 mS cm⁻¹ as the weight percentage of TBAI increased from 5.11 to 24.08 %. Beyond that, the conductivity dropped to 4.88 mS cm⁻¹ as the salt concentration increased to 29.57 wt%.

Fig. 1 Nyquist plots of selected blended PEO-PVA GPEs at 303 K



This trend can be explained by the ion-pair model. When small amount of salt is dissolved in the GPE, the ions can form a homogenous system in the GPE. In this condition, the ions are in the solvation state. Increasing the concentration of salts can increase the amount of mobile charge carriers and thus increase the conductivity of the GPE. Beyond 24.08 wt% TBAI, the σ of the GPE decreases, which may be due to the fact that the ions that contribute to the conductivity have changed from solvation state to contact ions [33].

In order to gain insight into the ionic transport, the ionic mobility (μ) and number density (n) of ions at

303 K for all samples have been calculated from the equations below [34]:

$$D = \frac{d^2}{\tau \delta^2} \quad (4)$$

$$\mu = \frac{eD}{k_B T} \quad (5)$$

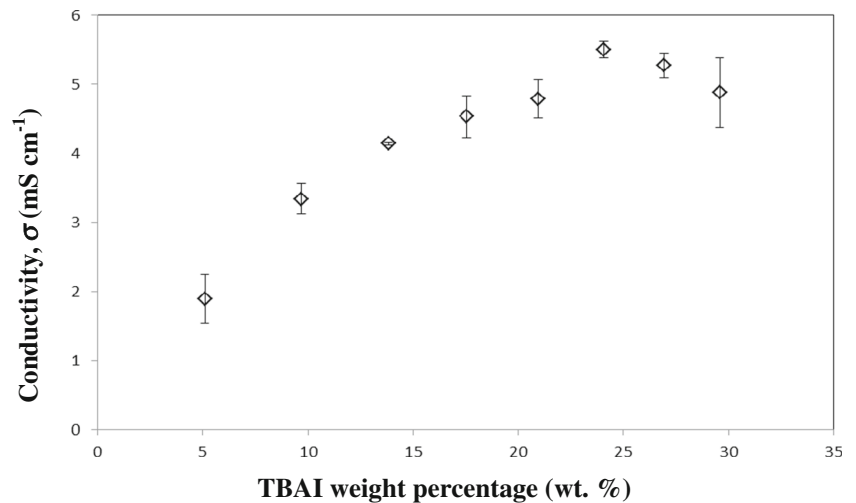
$$n = \frac{\sigma}{e\mu} \quad (6)$$

Here, D is the diffusion coefficient, $\tau = 1/\omega$ (ω is the angular frequency at which the spike cuts the real impedance axis in

Table 3 σ , p , k^{-1} , μ , n , and D for different composition of GPEs at 303 K

| Sample | σ (mS cm ⁻¹) | p (radian) | k^{-1} (F) | D (cm ² s ⁻¹) | n (cm ⁻³) | μ (cm ² V ⁻¹ s ⁻¹) |
|--------|---------------------------------|--------------|-----------------------|----------------------------------------|-------------------------|----------------------------------------------------------|
| A | 1.90 | 0.88 | 1.55×10^{-5} | 1.48×10^{-4} | 2.10×10^{18} | 5.66×10^{-3} |
| B | 3.34 | 0.87 | 1.99×10^{-5} | 2.26×10^{-4} | 2.41×10^{18} | 8.67×10^{-3} |
| C | 4.14 | 0.86 | 2.09×10^{-5} | 2.79×10^{-4} | 2.42×10^{18} | 1.07×10^{-2} |
| D | 4.54 | 0.87 | 2.52×10^{-5} | 1.61×10^{-4} | 4.58×10^{18} | 6.18×10^{-3} |
| E | 4.79 | 0.89 | 1.74×10^{-5} | 4.86×10^{-4} | 1.61×10^{18} | 1.86×10^{-2} |
| F | 5.50 | 0.89 | 1.75×10^{-5} | 1.15×10^{-3} | 7.81×10^{17} | 4.39×10^{-2} |
| G | 5.28 | 0.90 | 1.67×10^{-5} | 1.13×10^{-3} | 7.64×10^{17} | 4.31×10^{-2} |
| H | 4.88 | 0.88 | 1.63×10^{-5} | 1.28×10^{-3} | 6.19×10^{17} | 4.92×10^{-2} |

Fig. 2 Variation of ionic conductivity of electrolytes with TBAI concentration at 303 K



the Nyquist plot), $\delta = d/\lambda$, d is the half of sample thickness, k_B is the Boltzmann's constant, $\lambda = \epsilon' \epsilon_o A/k^{-1}$ is the thickness of the electrical double layer and A is the area of the sample, k^{-1} is obtained from the fitting of the experimental data using Eqs. (2) and (3), ϵ_o is the vacuum permittivity, and ϵ' is the dielectric constant of the GPE (taken at frequency 45 kHz from the ϵ' versus $\log \omega$ plot). Dielectric constant, ϵ' can be calculated from the equation below:

$$\epsilon' = \frac{Z''}{\omega(\epsilon_o A/t)(Z'^2 + Z''^2)} \tag{7}$$

The values of conductivity, capacitance, diffusion coefficient, ionic mobility, and number density of ion at 303 K are summarized in Table 3.

Based on Eq. (6), it can be understood that the increase in conductivity can be attributed to the increase in number density or mobility of mobile ions or increase in the product $n\mu$. The conductivity of the electrolyte is the highest at 24.08 wt% TBAI because the product of n and μ is the highest. According to Table 3, the number density of the mobile ion, n , increases continuously with increasing salt concentration from 5.11 wt% TBAI to 17.56 wt% TBAI. This increment in number density of mobile ions is due to the increase in the amount of salt added into the GPE. Further increase in salt concentration from 17.56 wt% TBAI to 29.57 wt% TBAI saw the decrease in number density of the mobile ions. This is due to the formation of the contact ions, which do not contribute to conductivity. On the other hand, the mobility of the charge carriers increased with increasing salt concentration from 5.11 wt% TBAI to 13.82 wt% TBAI but decreased at 17.56 wt% TBAI, where the number density of mobile ions is highest [35]. The decrement in the mobility is due to the

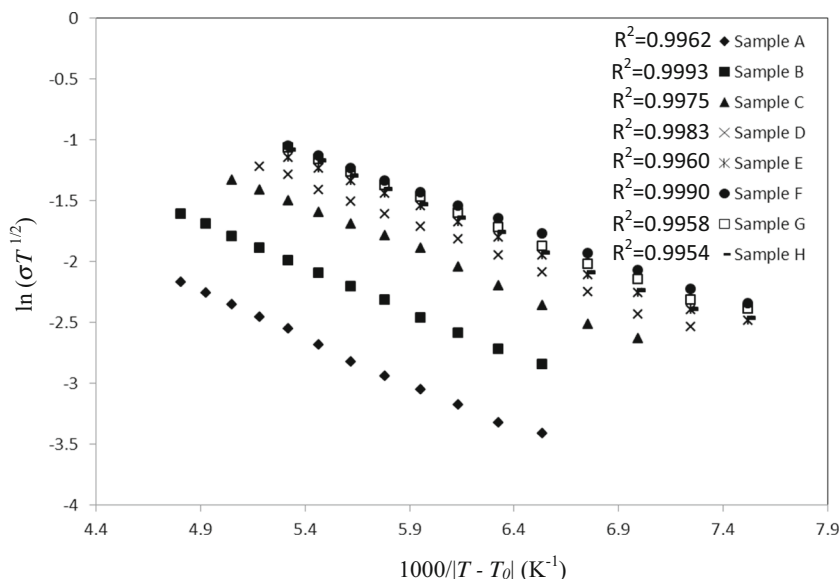
electrostatic hindrance between ions [36]. On further increasing the salt concentration up to 29.57 wt% TBAI, the mobility of charge carrier increases steeply, while the number density decreases. Hence, the mobility of the charge carriers is the dominating factor in the highest conductivity sample. The increase in mobility is caused by the formation of contact ions, which are electrically neutral, and thus substantially reduce the electrostatic hindrance [31]. Figure 3 shows the graph of $\ln(\sigma T^{1/2})$ against $1000 / |T - T_0|$ for all GPEs.

As can be seen from Fig. 3, the conductivity–temperature data show a straight line, indicating that the Vogel–Tammann–Fulcher (VTF) equation should be used to interpret the data. The VTF equation is given as follows:

$$\sigma = \frac{A}{T^{1/2}} \exp\left(-\frac{B}{k_B(T-T_o)}\right) \tag{8}$$

Here, σ is the conductivity of the sample, T is the absolute temperature, T_o is the ideal glass transition temperature at which the free volume vanishes and the ionic mobility goes to zero [37], A is a pre-exponential factor which is related to the number density of charge carriers, and B is the pseudo-activation energy of the ion transport related to the configurational entropy of the polymer chain [38]. B is directly proportional to activation energy [39]. The values of T_o , which are in the range 150 to 170 K, have been obtained by choosing the values that make the graph of $\ln(\sigma T^{1/2})$ versus $1000 / (T - T_o)$ closest to a linear line with regression coefficient, $R^2 \sim 1$. Table 4 lists the pseudo-activation energy and T_o values for the PEO-PVA-blended GPEs. The higher the conductivity of the sample, the lower the activation energy. From Table 4, it can be seen that the value of B decreases from 64 meV to a minimum value of 52 meV at 24.08 wt% TBAI as the conductivity

Fig. 3 The graphs of $\ln(\sigma T^{1/2})$ against $1000/|T - T_0|$ for all samples



increased. The value of B then increases to 57 meV as the conductivity decreased.

Figure 4 depicts the variation of number density and mobility of charge carriers with temperature for the highest conducting GPE. As can be observed from Fig. 4, the ionic mobility increased with temperature, while the number density of mobile ions decreased at elevated temperatures. The increase in mobility with temperature can be explained by free-volume model, which states that increasing temperature will increase the free volume in the polymer and thus enhances the mobility of the ions [40].

DSSC performance

The open-circuit voltage (V_{oc}) and short-circuit current density (J_{sc}) of DSSCs can be obtained directly from the J - V characteristics as shown in Fig. 5. The fill

factor (FF) and efficiency (η) of the cells have been calculated using the equations below [41]:

$$FF = \frac{J_{max} \times V_{max}}{J_{sc} \times V_{oc}} \tag{9}$$

$$\eta = \frac{J_{sc} \times V_{oc} \times FF}{P_{in}} \times 100\% \tag{10}$$

where J_{max} and V_{max} are the maximum current density and maximum voltage, respectively, at the point of maximum power output density. J_{sc} is the short-circuit current density, V_{oc} is the open-circuit voltage, and P_{in} is the incident light power density.

As shown in Eq. (10), the efficiency of DSSC is dependent on the J_{sc} , V_{oc} , and FF parameters. Generally, J_{sc} is related to the charge generation produced by dye absorption and charge transport in the electrolyte. Electron injection and recombination are also other factors that influence the J_{sc} . The V_{oc} is determined from the potential difference between the Fermi level of TiO_2 and redox potential in the electrolyte. On the other hand, FF value depends on the series and shunt resistances in DSSC [42]. The FF can be increased if the shunt resistance increased and/or series resistance decreased [43].

When the dye molecules (D) are excited and inject electrons into the conduction band of TiO_2 (D^+), they have to be restored by the redox mediators in the electrolyte as shown in Eq. (11).



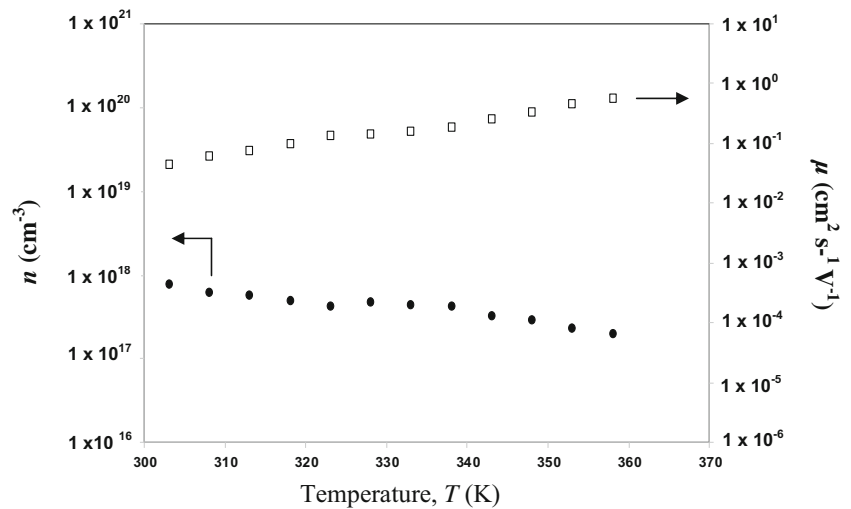
The triiodide, I_3^- , has to diffuse to the counter electrode and be reduced back to iodide, I^- , on accepting electrons at the counter electrode as shown in Eq. (12) for dye restoration (equation 11).



Table 4 Pseudo-activation energy, B , and T_0 for PEO-PVA-blended GPEs

| Sample | B (meV) | T_0 (K) |
|--------|-----------|-----------|
| A | 64 | 150 |
| B | 61 | 152 |
| C | 59 | 160 |
| D | 56 | 165 |
| E | 55 | 170 |
| F | 52 | 170 |
| G | 54 | 170 |
| H | 57 | 170 |

Fig. 4 Variation of number density and mobility of charge carrier with temperature for the highest conducting sample



The processes involved in Eqs. (11) and (12) have to be fast in order to obtain high efficiency. This is the reason why the tetrabutylammonium cation has been chosen in this work. Conductivity of the electrolytes is contributed by anions and cations. In this case, the cation is more bulky and larger than the anion. Therefore, the main contributor to conductivity is the anions. Moreover, anions complete the circuit by redox process. Bandara and co-authors [44] also agreed that the conductivity of GPE containing PAN, tetrahexylammonium iodide, and magnesium iodide is mainly attributed to iodide ions. Table 5 shows the J_{sc} , V_{oc} , FF , and η of the DSSCs with different GPEs.

It is evident that the DSSC with the highest conducting GPE (sample F), i.e., cell 6, exhibits the highest short-circuit current density and efficiency of 12.31 mA cm^{-2} and 5.36% , respectively. The efficiency of DSSCs increases from 2.99% (cell 1) to 5.36% (cell 6) and then decreases to 4.56% (cell 8). The high conductivity of GPE will facilitate the transportation of charge in the DSSC, while other factors remain unchanged. As can be observed from Table 5, the trends of J_{sc} and η follow the trend of conductivity and there is no much difference in the values of FF and V_{oc} . Fill factors and V_{oc} are observed in the range 0.57 to 0.66 and 0.64 to 0.66 V , respectively. The small

difference in V_{oc} values may be due to the changes in the Fermi level of TiO_2 .

Figure 6 shows the EIS spectra of the DSSCs measured under white light intensity of 100 mW cm^{-2} . The equivalent circuit of the Nyquist plots is shown in the inset of Fig. 6. The EIS spectra are fitted using the equivalent circuit (the inset of Fig. 6), and the fitting lines are shown in Fig. 6. The equation below shows the impedance of the equivalent circuit:

$$Z_{\text{total}} = R_s + \frac{R_{ce}}{1 + (j\omega)^m R_{ce} Q_{ce}} + \frac{R_{ct}}{1 + (j\omega)^n R_{ct} Q_{ct}} \quad (13)$$

Here, R_s is the sum of the sheet resistance of the FTO layer and contact resistances, j is the imaginary number, R_{ce} is the charge transfer resistance at the electrolyte/counter electrode interface, Q_{ce} is the constant phase element prefactor at the electrolyte/counter electrode interface, R_{ct} is the charge transfer resistance at the electrolyte/photoanode interface, Q_{ct} is the constant phase element prefactor at the electrolyte/photoanode interface, and m and n are the indexes that indicate the non-ideal capacitance property of Q_{ce} and Q_{ct} , respectively [45, 46].

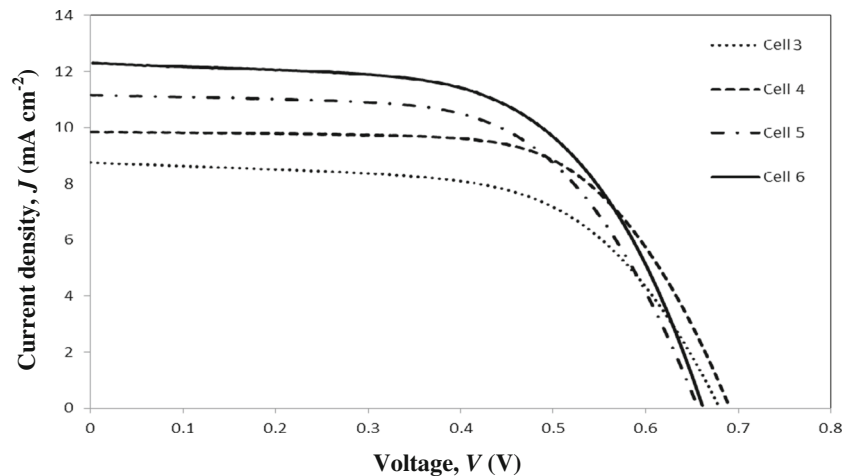
Table 5 J_{sc} , V_{oc} , FF , and η of the DSSCs with different GPEs

| Cell | GPE sample | J_{sc} (mA cm^{-2}) | V_{oc} (V) | FF | η (%) |
|------|------------|----------------------------------|--------------|------|------------|
| 1 | A | 7.31 | 0.65 | 0.63 | 2.99 |
| 2 | B | 8.79 | 0.66 | 0.60 | 3.48 |
| 3 | C | 10.82 | 0.65 | 0.57 | 4.04 |
| 4 | D | 11.21 | 0.64 | 0.59 | 4.21 |
| 5 | E | 11.26 | 0.65 | 0.61 | 4.46 |
| 6 | F | 12.31 | 0.66 | 0.66 | 5.36 |
| 7 | G | 12.28 | 0.65 | 0.65 | 5.19 |
| 8 | H | 11.34 | 0.65 | 0.62 | 4.56 |

Table 6 R_s , R_{ct} , Q_{ct} , n , and τ of the DSSCs

| Cell | R_s (Ω) | R_{ct} (Ω) | Q_{ct} (mS s^n) | n | τ (ms) |
|------|--------------------|-----------------------|------------------------------|------|-------------|
| 1 | 17.94 | 34.00 | 2.30 | 0.80 | 41.35 |
| 2 | 17.26 | 33.00 | 2.39 | 0.79 | 40.15 |
| 3 | 18.20 | 32.00 | 3.13 | 0.71 | 39.13 |
| 4 | 16.26 | 30.20 | 3.11 | 0.72 | 37.43 |
| 5 | 18.37 | 33.50 | 2.45 | 0.77 | 38.89 |
| 6 | 16.94 | 34.30 | 2.61 | 0.75 | 40.05 |
| 7 | 15.79 | 33.70 | 2.60 | 0.76 | 40.62 |
| 8 | 18.38 | 34.50 | 2.30 | 0.79 | 40.46 |

Fig. 5 The J - V characteristics for selected DSSCs with different GPEs



Under bias voltage near the V_{oc} , it is possible to see three semicircles in the Nyquist plot. The first one in the high-frequency region corresponds to the charge transfer process at the Pt/electrolyte interface, the second semicircle in intermediate frequency is related to the chemical capacitance and charge transfer resistance at the TiO_2 /electrolyte interface, and the third one in the low-frequency region is ascribed to the diffusion of triiodide ion in the electrolyte [46]. However, there are only two depressed semicircles observed in the Nyquist plots in this work (Fig. 6). From Fig. 6, it can be seen that R_{ce} is almost same for all cells (first semicircle in the high-frequency region).

Table 6 lists the values of R_s , R_{ct} , Q_{ct} , n , and electron lifetime (τ) of the DSSCs. As can be seen from Table 6, there is no significant change in the values of R_s , which are in the range of 15.79 to 18.38 Ω . This is because same FTO substrates and same procedure are used in fabricating the DSSCs in this work. According to literature [47], Q_{ct} represents generalized electrochemical capacitance to account for some frequency dispersion present in the impedance spectrum [47]. As observed in Table 6, the values of n are in the range from 0.71 to 0.80, which implies the existence of non-ideal capacitance properties at the TiO_2 /electrolyte interface.

Electron lifetime (τ) can be calculated using the equation below [45, 48]:

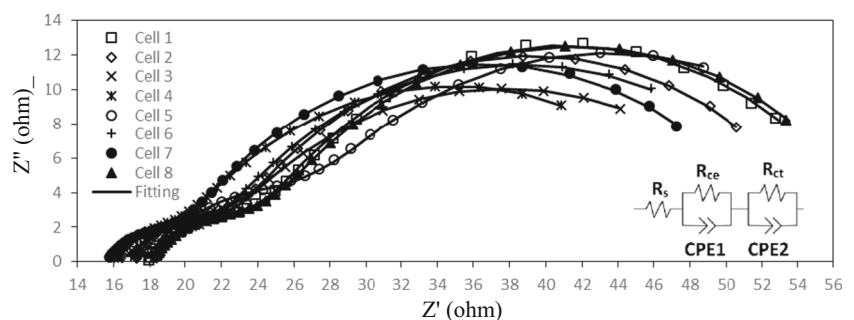
$$\tau = (Q_{ct}R_{ct})^{1/n} \quad (14)$$

The smaller is the electron lifetime, the higher is the recombination rate of electron with triiodide and dye cation. It is evident in Table 6 that there are no much changes in the values of R_{ct} and τ , which are in the range of about 30 to 34 Ω and 37 to 41 ms, respectively. This indicates that the variation of the TBAI concentration has little effect on the charge transfer resistance and the recombination of the electrons with triiodide ions. The highest efficiency exhibited by cell 6 is due to its high conductivity of the GPE. Therefore, it can be concluded that the conductivity of GPEs is the only factor that is influencing the efficiency of DSSCs in this system.

Conclusions

Blended gel polymer electrolytes containing PEO, PVA, TBAI, iodine, EC, and DMSO have been prepared and applied in DSSCs. The highest product of number density and ionic mobility gives the highest value of conductivity. The

Fig. 6 EIS spectra of the DSSCs under white light illumination. The inset shows the equivalent circuit of the EIS spectra



PEO-PVA-based GPE with the highest conductivity of 5.50 mS cm^{-1} was obtained for the composition of 7.02 wt% PVA, 7.02 wt%, PEO 30.11 wt%, EC 30.11 wt%, DMSO 24.08 wt%, and TBAI 1.66 wt% iodine crystals (I_2). The conductivity–temperature relationship of the GPEs follows VTF behavior. The highest efficiency of 5.36 % is obtained for DSSC with the highest conducting GPE.

Acknowledgments The authors would like to thank the Ministry of Higher Education for the FRGS grant No. FP007-2013B and University of Malaya for grant No. RP003-13AFR.

References

- O'Regan B, Gratzel M (1991) A low-cost, high-efficiency solar cell based on dye-sensitized colloidal TiO_2 films. *Nature* 353(6346): 737–740
- Poudel P, Qiao Q (2014) Carbon nanostructure counter electrodes for low cost and stable dye-sensitized solar cells. *Nano Energy* 4(0): 157–175
- Ahmad I, Khan U, Gun'ko YK (2011) Graphene, carbon nanotube and ionic liquid mixtures: towards new quasi-solid state electrolytes for dye sensitised solar cells. *J Mater Chem* 21(42): 16990–16996
- Snaith HJ (2010) Estimating the maximum attainable efficiency in dye-sensitized solar cells. *Adv Funct Mater* 20(1):13–19
- Shockley W, Queisser HJ (1961) Detailed balance limit of efficiency of p-n junction solar cells. *J Appl Phys* 32(3):510–519
- Grätzel M (2003) Dye-sensitized solar cells. *J Photochem Photobiol C: Photochem Rev* 4(2):145–153
- Bach U, Lupo D, Comte P, Moser JE, Weissortel F, Salbeck J, Spreitzer H, Gratzel M (1998) Solid-state dye-sensitized mesoporous TiO_2 solar cells with high photon-to-electron conversion efficiencies. *Nature* 395(6702):583–585
- Wu JH, Lan Z, Lin JM, Huang ML, Hao SC, Sato T, Yin S (2007) A novel thermosetting gel electrolyte for stable quasi-solid-state dye-sensitized solar cells. *Adv Mater* 19(22):4006–4011
- Chen C-L, Teng H, Lee Y-L (2011) In situ gelation of electrolytes for highly efficient gel-state dye-sensitized solar cells. *Adv Mater* 23(36):4199–4204
- Rika AA, Rahman MYA, Salleh MM (2009) Preparation and characterization of PAN based solid polymeric electrolyte for dye-sensitized solar cells. *Phys B Condens Matter* 404(8–11):1359–1361
- Anandan S, Pitchumani S, Muthuraaman B, Maruthamuthu P (2006) Heteropolyacid-impregnated PVDF as a solid polymer electrolyte for dye-sensitized solar cells. *Sol Energy Mater Sol Cells* 90(12):1715–1720
- Theerthagiri J, Senthil RA, Buraidah MH, Madhavan J, Arof AK (2015) Effect of tetrabutylammonium iodide content on PVDF-PMMA polymer blend electrolytes for dye-sensitized solar cells. *Ionics* 21(10):2889–2896
- Theerthagiri J, Senthil RA, Ali@Buraidah MH, Madhavan J, Mohd Arof AK (2015) Studies of solvent effect on the conductivity of 2-mercaptopyridine-doped solid polymer blend electrolytes and its application in dye-sensitized solar cells. *J Appl Polym Sci* 132(35):42489
- Chen K-F, Liu C-H, Huang H-K, Tsai C-H, Chen F-R (2013) Polyvinyl butyral-based thin film polymeric electrolyte for dye-sensitized solar cell with long-term stability. *Int J Electrochem Sci* 8:3524–3539
- Kang J, Li W, Wang X, Lin Y, Xiao X, Fang S (2003) Polymer electrolytes from PEO and novel quaternary ammonium iodides for dye-sensitized solar cells. *Electrochim Acta* 48(17):2487–2491
- Tiautit N, Puratane C, Panpinit S, Saengsuwan S (2014) Effect of SiO_2 and TiO_2 nanoparticles on the performance of dye-sensitized solar cells using PVDF-HFP/PVA gel electrolytes. *Energy Procedia* 56(0):378–385
- Wang X, Zhang Y, Xu Q, Xu J, Wu B, Gong M, Chu J, Xiong S (2015) A low-cost quasi-solid DSSC assembled with PVDF-based gel electrolyte plasticized by PC-EC & electrodeposited Pt counter electrode. *J Photochem Photobiol A Chem* 311:112–117
- Ren Y, Zhang Z, Fang S, Yang M, Cai S (2002) Application of PEO based gel network polymer electrolytes in dye-sensitized photoelectrochemical cells. *Sol Energy Mater Sol Cells* 71(2): 253–259
- Yang H, Huang M, Wu J, Lan Z, Hao S, Lin J (2008) The polymer gel electrolyte based on poly(methyl methacrylate) and its application in quasi-solid-state dye-sensitized solar cells. *Mater Chem Phys* 110(1):38–42
- Aram E, Ehsani M, Khonakdar HA (2015) Improvement of ionic conductivity and performance of quasi-solid-state dye sensitized solar cell using PEO/PMMA gel electrolyte. *Thermochim Acta* 615:61–67
- Arof AK, Aziz MF, Noor MM, Careem MA, Bandara LRAK, Thotawatthage CA, Rupasinghe WNS, Dissanayake MAKL (2014) Efficiency enhancement by mixed cation effect in dye-sensitized solar cells with a PVdF based gel polymer electrolyte. *Int J Hydrog Energy* 39(6):2929–2935
- Higashino T, Imahori H (2015) Porphyrins as excellent dyes for dye-sensitized solar cells: recent developments and insights. *Dalton Trans* 44:448
- Sandoval C, Castro C, Gargallo L, Radic D, Freire J (2005) Specific interactions in blends containing chitosan and functionalized polymers. *Molecular dynamics simulations. Polymer* 46(23):10437–10442
- Kuila T, Acharya H, Srivastava SK, Samantaray BK, Kureti S (2007) Enhancing the ionic conductivity of PEO based plasticized composite polymer electrolyte by LaMnO_3 nanofiller. *Mater Sci Eng B* 137(1–3):217–224
- Jia Y-T, Gong J, Gu X-H, Kim H-Y, Dong J, Shen X-Y (2007) Fabrication and characterization of poly (vinyl alcohol)/chitosan blend nanofibers produced by electrospinning method. *Carbohydr Polym* 67(3):403–409
- Yang C-C, Wu GM (2009) Study of microporous PVA/PVC composite polymer membrane and its application to MnO_2 capacitors. *Mater Chem Phys* 114(2–3):948–955
- Joge P, Kanchan DK, Sharma P, Niral G (2013) Effect of nanofiller on electrical properties of PVA-PEO blend polymer electrolyte. *India J Pure Appl Phys* 51:350
- Abd El-kader FH, Hakeem NA, Elashmawi IS, Ismail AM (2013) Structural, optical and thermal characterization of ZnO nanoparticles doped in PEO/PVA blend films. *Aust J Basic Appl Sci* 7(10): 608–619
- Kapil M, Lata S (2013) A review: residual solvents and various effective gas chromatographic techniques in the analysis of residual solvent. *Int J Pharm Res Rev* 2(10):25–40
- Rajendran S, Babu RS, Sivakumar P (2007) Effect of salt concentration on poly (vinyl chloride)/poly (acrylonitrile) based hybrid polymer electrolytes. *J Power Sources* 170(2):460–464
- Arof AK, Naeem M, Hameed F, Jayasundara WJMJSR, Careem MA, Teo LP, Buraidah MH (2014) Quasi solid state dye-sensitized solar cells based on polyvinyl alcohol (PVA) electrolytes containing I⁻/I⁻³ redox couple. *Opt Quant Electron* 46(1):143–154
- Ramya CS, Selvasekarapandian S, Hirankumar G, Savitha T, Angelo PC (2008) Investigation on dielectric relaxations of PVP–

- NH₄SCN polymer electrolyte. *J Non-Cryst Solids* 354(14):1494–1502
33. Wu J, Lan Z, Wang D, Hao S, Lin J, Huang Y, Yin S, Sato T (2006) Gel polymer electrolyte based on poly(acrylonitrile-co-styrene) and a novel organic iodide salt for quasi-solid state dye-sensitized solar cell. *Electrochim Acta* 51(20):4243–4249
 34. Bandara TMWJ, Mellander BE (2011) Evaluation of mobility, diffusion coefficient and density of charge carriers in ionic liquids and novel electrolytes based on a new model for dielectric response. In: Alexander K (ed) *Ionic liquids: theory, properties, new approaches*. InTech, Croatia p383.
 35. Bandara TMWJ, Dissanayake MAKL, Albinsson I, Mellander BE (2011) Mobile charge carrier concentration and mobility of a polymer electrolyte containing PEO and Pr₄N⁺I⁻ using electrical and dielectric measurements. *Solid State Ionics* 189(1):63–68
 36. Oh B, Jung WI, Kim D-W, Rhee HW (2002) Preparation of UV curable gel polymer electrolytes and their electrochemical properties. *Bull Kor Chem Soc* 23(5):5
 37. Jing G, Zhen-Li G, Xiao-Li Y, Shu G, Zhong-Liang Z, Bo W (2012) Investigation of the free volume and ionic conducting mechanism of poly(ethylene oxide)-LiClO₄ polymeric electrolyte by positron annihilating lifetime spectroscopy. *Chin Phys B* 21(10):107803
 38. Saikia D, Pan Y-C, Kao H-M (2012) Synthesis, multinuclear NMR characterization and dynamic property of organic-inorganic hybrid electrolyte membrane based on alkoxysilane and poly(oxyalkylene) diamine. *Membranes* 2(2):253
 39. Vila J, Ginés P, Pico JM, Franjo C, Jiménez E, Varela LM, Cabeza O (2006) Temperature dependence of the electrical conductivity in EMIM-based ionic liquids: evidence of Vogel–Tamman–Fulcher behavior. *Fluid Phase Equilib* 242(2):141–146
 40. Sanchez Garcia MD, Lagaron JM (2012) 12—Nanocomposites for food and beverage packaging materials. In: Huang Q (ed) *Nanotechnology in the food, beverage and nutraceutical industries*. Woodhead Publishing, pp 335–361.
 41. Hafez H, Lan Z, Li Q, Wu J (2010) High efficiency dye-sensitized solar cell based on novel TiO₂ nanorod/nanoparticle bilayer electrode. *Nanotechnol Sci Appl* 3:45–51
 42. Guliani R, Jain A, Kapoor A (2012) Exact analytical analysis of dye-sensitized solar cell: improved method and comparative study. *Open Renewable Energy J* 5:49–60
 43. Yang R-Y, Chen H-Y, Lai F-D (2012) Performance degradation of dye-sensitized solar cells induced by electrolytes. *Adv Mater Sci Eng* 2012:4
 44. Bandara TM, Dissanayake MA, Jayasundara WJ, Albinsson I, Mellander BE (2012) Efficiency enhancement in dye sensitized solar cells using gel polymer electrolytes based on a tetrahexylammonium iodide and MgI₂ binary iodide system. *Phys Chem Chem Phys* 14(24):8620–8627
 45. Pugliese D (2014) New insights in dye-sensitized solar cells: novel nanostructured photoanodes, metal-free dye, quasi-solid electrolytes and physics-based modeling. Politecnico di Torino, Turin
 46. Sarker S, Ahammad AJS, Seo HW, Kim DM (2014) Electrochemical impedance spectra of dye-sensitized solar cells: fundamentals and spreadsheet calculation. *Int J Photoenergy* 2014:17
 47. Lamberti A, Sacco A, Bianco S, Quaglio M, Manfredi D, Pirri CF (2013) Enhancement of electron lifetime in dye-sensitized solar cells using anodically grown TiO₂ nanotube/nanoparticle composite photoanodes. *Microelectron Eng* 111:137–142
 48. Jun HK, Careem MA, Arof AK (2014) Investigation of multilayered quantum dot-sensitized solar cells with different Zn chalcogenide passivation layers. *J Appl Electrochem* 44(9):977–988